Imaging and quantifying the biological uptake and distribution of nanoplastics using a dual-functional model material

Mingjiu Liu[1,2], Anupam Das[1], Nubia Zuverza[3], Jason White[3], Huiyuan Guo*[1,2]

1 Department of Chemistry, State University of New York at Binghamton, Binghamton, NY, 13902, USA

2 Department of Material Science and Engineering, State University of New York at Binghamton, Binghamton, NY, 13902, USA

3 Department of Analytical Chemistry, The Connecticut Agricultural Experiment Station, New Haven, CT, 06511, USA

*Corresponding Author: Guo, Huiyuan (hguo@binghamton.edu)

Abstract

Nanoplastics (NPs) are invisible to human eyes yet pose significant concerns to human health due to their wide environmental presence and high potential for biological uptake, transport, and accumulation. Conventional analytical methods suffer from low accuracy and precision in NP detection due to their limited reliability and quantitative ability. To address these challenges, we developed a dual-functional model NP that allows for *in-situ* imaging by surface-enhanced Raman spectroscopy (SERS) and *ex-situ* quantification by inductively coupled plasma-mass spectrometry (ICP-MS). In this study, the model NP has a core-shell structure with Raman reporter-functionalized gold nanoparticles as the core and a layer of plastic as the shell. The gold core can enhance the Raman reporter signals and make model PS detectable, which can be used to visualize the uptake of the model NP in plant tissue by SERS. Meanwhile, the model NP particle numbers in the collected plants can be quantified by ICP-MS based on the presence of gold in the core. The model PS demonstrated stability in structure, size, and surface charges over one year, with no indication of chemical leaching. In this study, garlic plants were used as our experimental matrix to evaluate the potential of the dual-functional model PS for application in living organisms. Our aim was to determine whether the model PS in the garlic plants could be effectively quantified and qualified by SERS and ICP-MS. Garlic plants were grown in various concentrations of model NP suspensions for a 30-day period. The results showed that the NP uptake was concentration-dependent with higher concentrations of model NP leading to higher uptake by the garlic roots. The study also investigated the changes in NP uptake over time, showing that longer NP exposure resulted in more NP uptake in garlic roots. The study also demonstrated the effective coordination between SERS and ICP-MS. In cases where SERS had limitations in detecting the presence of model PS, ICP-MS proved capable of facilitating

detection in garlic tissue. This study demonstrates the potential use of this dual-functional model NP for studying NP behavior with SERS and ICP-MS in living organisms, which holds significant implications for better understanding their impact on crops for future studies.

Keywords: SERS, polystyrene nanoplastics, in-situ confocal Raman imaging, ICP-MS quantification

Graphical Abstract
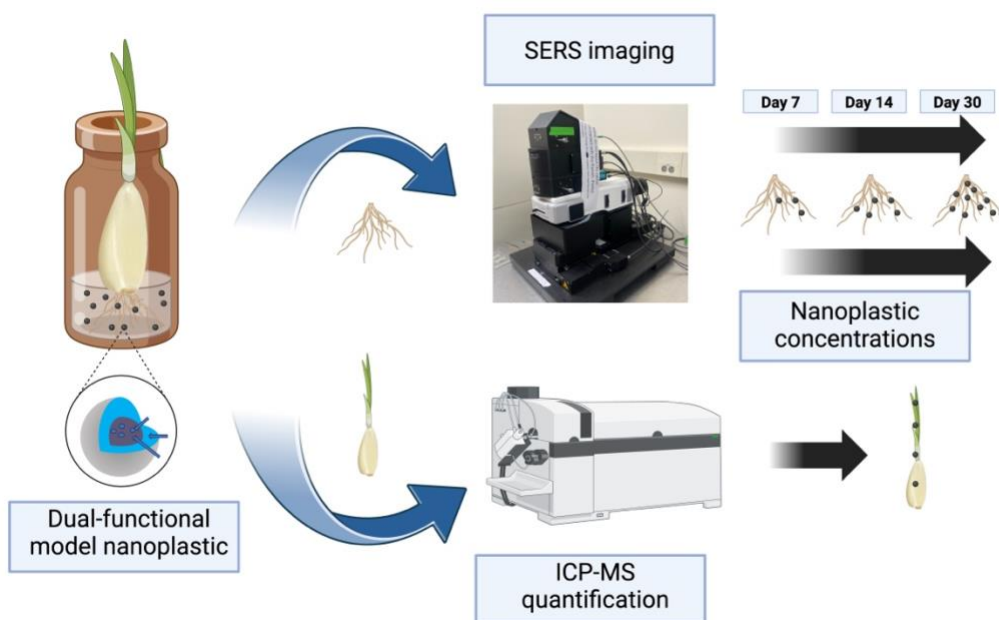
Created with BioRender.com

1. Introduction

Plastics are highly demanded in human's daily life and numerous applications of plastics are used nowadays and every day. Including fields such as agriculture,[1] healthcare,[2] construction,[3] packaging,[4] and textiles,[5] plastics find widespread use in various sectors.[6] Massive amounts of plastics have the potential to be released into the environment due to the broad applications and a low recycling rate.[7,8] When entering the environment, plastics can undergo degradation into smaller pieces through certain processes such as mechanical abrasion,[9] UV exposure,[10] and biological degradation.[11,12] They can break down the larger plastics into tiny particles measuring 1 to 100 nm, which are defined as nano plastics (NPs).[13] The presence of a large number of NPs has been identified in the soil and surface water,[14] and it has been proved that NPs are accumulating in the environment.[15] The concern is that NPs can contaminate irrigation water, leading to the contamination of crops with NPs. According to a recent study, it has been found that NPs can circulate in the environment and accumulate in the plants that humans consume.[16] The introduction of NPs into the food chain can affect food safety and human health due to the toxicity of these NPs.[17]

Given the presence of NPs in surface water, there is a high likelihood that crops may come into contact with NPs through root or foliar contact during irrigation. In fact, the levels of plastic particle contamination in terrestrial ecosystems can be 4-23 times higher than those found in marine systems, as per studies.[18,19] However, NP contamination in terrestrial ecosystems has been overlooked before, only gaining attention in the last few years. A recent study revealed that plant roots can uptake NPs, leading to their accumulation within the plants.[20] Another study

discovered the capability of NPs to translocate within plants. The initial contamination occurred through foliar contact on the leaves, and subsequently, the NPs were transported to the roots.[21] Should crop seeds become contaminated with NPs, the contamination is likely to extend to the roots, stems, and leaves of the plants.[22] Furthermore, it has been found the accumulation of NPs could have a significant impact on the growth and development of plants.[23] This has made people more interested, especially when it comes to improving agricultural yield. To identify NPs in plants, various techniques are commonly used, with microscopic and light scattering methods being among the most common techniques for qualitative detection. These methods include scanning electron microscopy (SEM), transmission electron microscopy (TEM), fluorescence microscopy (FM), and dynamic light scattering (DLS). Polystyrene (PS) has been identified as the most prevalent NP in various ecosystems and is the most detected type within the food chain.[24] In researching the uptake and distribution of NPs in plants, many studies have used fluorescent dye-labeled PS NPs as a model to simulate the behavior of NPs within the plant.[22,23] However, one of the drawbacks of using fluorescent dye-labeled NPs is the negative environmental impact. The introduction of fluorescent dye-labeled NPs into ecosystems may have unintended environmental consequences. Secondly, it might alter the surface properties of NPs, affecting their interactions with plants and the environment in ways that differ from unlabeled NPs.(**Fig. S3**) Additionally, the release of fluorescent dye from NPs could impact the accuracy of results and lead to false signals.[25] When studying the distribution of NPs in plants, uncertainty arises regarding whether plants uptake the dye or the NPs. Studies have revealed that NPs can negatively influence crop growth.[26,27] However, when using dye-labeled NPs, it remains uncertain whether it is the dye or the NPs themselves that have an impact. Lastly, biological autofluorescence has the potential to interfere with the fluorescent dye.[28,29] A novel model of

NPs without fluorescent dye is needed to overcome these limitations. However, microscopic imaging techniques can only qualitatively analyze a small fraction of plant tissue. The result is not able to represent the whole plant. Developing a non-destructive method to detect NPs in plants poses a challenge. For novel detection methods, some radioisotope techniques have been previously performed to study the distribution and fate of plastics in crop plants, but radioactive substances have always been a concern when dealing with living organism samples.[30] The challenge is to find a method to real-time detect NPs in living biological samples without damaging the tissues. A detection method model capable of both quantitative and qualitative measurement of NPs is essential for studying the uptake mechanism and tracing the behavior of NPs in biological samples.

The objective of this study is to develop a dual-model PS NP material that doesn't contain fluorescence dye capable of enabling in situ quantification and qualification detection in plants. This material enables qualitative imaging and quantitative assessment of the biological uptake and transport of NPs in plants, as well as their impact on plant growth. Garlic plants were specifically chosen and exposed to model NP suspension for this research, as garlic is a widely consumed food by humans. Subsequent steps involve imaging and quantifying the model NPs in garlic plants by model detection methods. A new analytical model of NP detection was developed in this study. This detection model combines Surface-Enhanced Raman Spectroscopy (SERS) with Inductively Coupled Plasma Mass Spectrometry (ICP-MS). SERS was used for imaging NPs in garlic plants, providing insights into the presence of NPs within different parts of garlic plants. Furthermore, ICP-MS was used to quantitatively assess the model NP particle numbers in different parts of garlic plants, including the roots and the upper part of garlic plants. This serves to validate the SERS imaging results and provide more accurate quantitative data that

may not be detectable through SERS alone. This combination of analytical techniques facilitates the investigation of the uptake and distribution of model NPs in garlic plants. [31]The reliable SERS imaging approach makes deep tissue detection possible and can also study the behavior and impact of NPs on biological samples with model NPs in the future. Using the dual-model material and detection method to detect model NPs enables a comprehensive understanding of the uptake and distribution of NPs in edible plants. This model material and detection method is suitable for future studies of NPs in biological samples. This knowledge contributes to assessing the potential risks to food safety and human health.

2. Materials and methods

2.1 Materials

The synthesis of the model NP utilized the same materials and protocol as described in our previous study.[32] All chemicals were purchased from either Fisher Chemical or Sigma Aldrich.

2.2 Preparation of NPs

In brief, the model NPs feature a core-shell structure, with a gold nanoparticle (nAu) at the core. A SERS nanotag called 4-Mercaptobenzoic acid (4-MBA) is labeled on the gold core. Surrounding the gold core is a PS shell, forming the core-shell structure of the model PS NP. The initial step involves producing citrate-stabilized gold seeds using sodium citrate and $HAuCl_4 \cdot 3H_2O$ which are then used for further synthesis of nAu. Next, the gold seeds are added to an HCl solution and mixed with $HAuCl_4 \cdot 3H_2O$. Simultaneously, the freshly prepared ascorbic acid solution is added, allowing the reaction to proceed for 30 seconds while stirring with a magnetic stir bar. The suspension is then centrifuged to remove the supernatant and stored in the refrigerator (4 °C) for future use.

The second step entails labeling the gold core with the SERS nanotag. The gold enhances the nanotag signal, allowing the NP to be detected by Raman spectroscopy. 4-MBA was chosen for its sharp characteristic SERS peak and ability to form covalent bonds with gold, preventing leakage. First, add NaOH to the nAu suspension to prevent aggregation. Then, add 4-MBA in ethanol to the suspension and allow it to incubate for 10 minutes. To remove excess 4-MBA molecules, the suspension is centrifuged. The supernatant is discarded, and the particles are resuspended in ultrapure water.

To ensure that the model NP retains its plastic properties, we coated the nAu with a PS layer. This ensures that the behavior of the model NP remains consistent with that of plastic. Using a bottom-up synthesis method, we used a wet chemical approach to cat the PS layer. The size of the model NPs can be controlled by extending the reaction time. The final model NPs were centrifuged and resuspended in ultrapure water.

2.3 Garlic plant cultivation and NP exposure

To evaluate the possibility of using this dual-functional model NPs and detection method, we selected garlic plants as the matrix for our study. To start the study, garlic bulbs with peels were purchased from a local grocery store. The garlic bulbs were then peeled and grown in varying concentrations of NP suspension until they generated roots and shoots. Subsequent steps involve imaging and quantifying the model NPs in garlic plants by model detection methods.

Fresh garlic bulbs were purchased from a nearby grocery store. First, 20 cloves were peeled and subsequently placed into 20 20 mL Amber glass vials. Cloves were selected based on their similar weights to ensure accuracy in the experiment. To expose garlic to NPs, 2 mL of diluted NP suspensions was initially added on day 1 to each vial. The exposure concentration of PS NP suspensions was determined according to the actual concentration observed in surface water

systems. In surface water systems, a study detected the highest concentration of PS NPs at 1.02×10^{15} particles/mL.[33] However, concerning the uptake of PS NP by plants from irrigation water, the concentration could potentially be exponentially lower. Considering the detection limit of SERS and its relevance to agriculture, we aim to maintain the concentration of PS NP suspensions as low as possible while still being detectable by SERS. The concentrations of NP suspensions included 0 particles/mL, 2×10^{9} particles/mL, 2×10^{10} particles/mL, and 2×10^{11} particles/mL. Each concentration was subjected to five replicates for experimental validity. The garlic plant samples were placed and grown inside a clean chamber to provide a well-ventilated environment. To ensure enough light for growth, a sunlight simulator was used, providing 8 hours of light daily to promote growth. 1 mL of ultrapure water was added to each vial every other day to ensure sufficient watering for an entire 30-day growth period. To assess the influence of NPs on garlic plant growth, the mass of each garlic plant on day 1 and day 30 was recorded for comparison. The root germination, and shoot germination rates of garlic plants were recorded as time progressed for 30 days to assess the influence of NPs on garlic plants' germination.

Another batch of garlic plants was cultivated under different conditions: Instead of adding PS NP suspension only once on day 1, we added their proper concentrations of 2 ml PS NP suspensions into their respective vials on day 1, and 1 mL PS NP suspensions on day 2, 4, and 6 (a total of four times). Additionally, 1 mL of ultrapure water was added every other day starting from day 8 until day 30. The varied exposure conditions aimed to replicate real-world irrigation scenarios, allowing for comparison with the single exposure group to assess potential differences.

2.4 Qualitative Confocal Raman Microscopy Imaging

We used an Alpha 300R Raman spectroscope from WITec for imaging. The confocal microscope is equipped with a 785 nm laser and offers magnification options of 10x, 50x, and 100x. SERS imaging of model NP in/on garlic samples is performed using an auto-scanning system, which utilizes motorized X-Y scanning and Z-focusing functions. The Raman mappings and spectra of model NPs are processed using the software Project Five+. We are able to observe the presence and distribution of NPs in garlic samples by using this technique. The scanning settings such as laser power, scanning step size, and integration time are adjusted prior to testing to ensure that the energy generated by the gold core does not damage the garlic sample tissue.

2.5 Quantitative detection of NPs with ICP-MS

To precisely assess the concentration of NPs in different segments of garlic plants (roots, and upper part), we used ICP-MS for accurate quantitative detection, enabling us to investigate the uptake and distribution of NPs within the garlic plants. Due to the composition of model PS NPs, it requires two acid digestion steps before starting the ICP-MS analysis. To break down the PS layer of the model PS NPs and garlic tissue, we used the Anton Paar Multiwave PRO acid digester with serial number 82459284, operating on instrument software version 3.20.10645.6. The digestion process was carried out separately for the root, and upper part segments. Each segment was placed into the digestion vessel along with an acid mixture consisting of 8 ml HNO_3 and 1 ml H_2SO_4, and then subjected to digestion for 7 hours at 180°C. After undergoing acid digestion in the acid digester, the sample volume was approximately 1 mL. Following this, to digest the gold core of the model PS NPs for ICP-MS analysis, it was further digested with 1 mL of aqua regia at room temperature for 2 hours. In preparation for ICP-MS analysis, 0.5 mL of the digested sample was diluted with 4.5 mL of ultrapure water to achieve an acid concentration

of 5%. Prior to analysis by ICP-MS, the samples underwent filtration using Biomed Scientific's Syringe Filters Nylon with a 25mm diameter and a pore size of 0.45 micrometers. This analytical technique is highly sensitive, allowing for precise determination of gold content with detection limits ranging from parts per trillion (ppt) to parts per billion (ppb). It provides valuable insights into the concentration and distribution of gold within each segment of the garlic plants.

3. Results and discussion

We developed a dual-functional model PS NP that enables qualitative visualization using SERS imaging and quantitative assessment of PS NP concentrations through ICP-MS. Utilizing this dual-functional model NP enables in situ imaging of biological samples without damaging. Due to the presence of gold in the model NPs, ICP-MS quantification is also feasible when the SERS detection limit is reached. To evaluate the application of the model NPs, we used garlic plants as a matrix to test the model NPs. Specifically, we exposed the garlic plants to the model NPs for a period of time and utilized the SERS and ICP-MS analysis model to study the uptake and distribution of NPs in different parts of the garlic plants over time. The model PS NPs were characterized using Dynamic Light Scattering (DLS, Zetasizer Nano ZS, Malvern Instruments), Transmission Electron Microscopy (TEM) (JEOL JEM 2100F), and Ultraviolet-Visible spectroscopy (UV-Vis, HP/Agilent 8453).

3.1 Model PS NPs stability characterization

TEM results confirmed the core-shell structure of the model NP featuring a gold crore at the center and a PS shell surrounding it. The diameter was measured to be 61.0 ± 0.66 nm, comprising a 33.6 ± 0.65 nm gold core and a 13.7 ± 0.18 nm PS layer. Raman results demonstrated that the gold core significantly enhances the Raman reporter signal. A redshift of the maximum absorption peak in the UV-Vis spectra indicated that the PS coating was

successfully applied to the gold core. **Figure 1a** illustrates the structure of the model PS NPs, which feature a core-shell structure. There is a gold core at the center, which is tagged with 4-MBA as the SERS nanotags. Surrounding the core is a PS shell to simulate the PS surface properties. The presence of gold significantly amplifies the SERS nanotags signals, enhancing Raman signals exponentially and making it more accurate and easier to detect.

Furthermore, we assessed the stability of the model NPs by comparing TEM characterization images of the freshly prepared model NPs (**Fig. 1c**) and 12 months later after synthesis (**Fig. 1d**). The results indicate the stability of the model NPs that the model NPs maintained their core-shell structure, with no breakage observed. These two TEM images were taken from different batches of samples, the consistent average particle diameter and the structure demonstrated the reproducibility of this synthesis method. To evaluate the stability of the model NP suspension and determine if it would
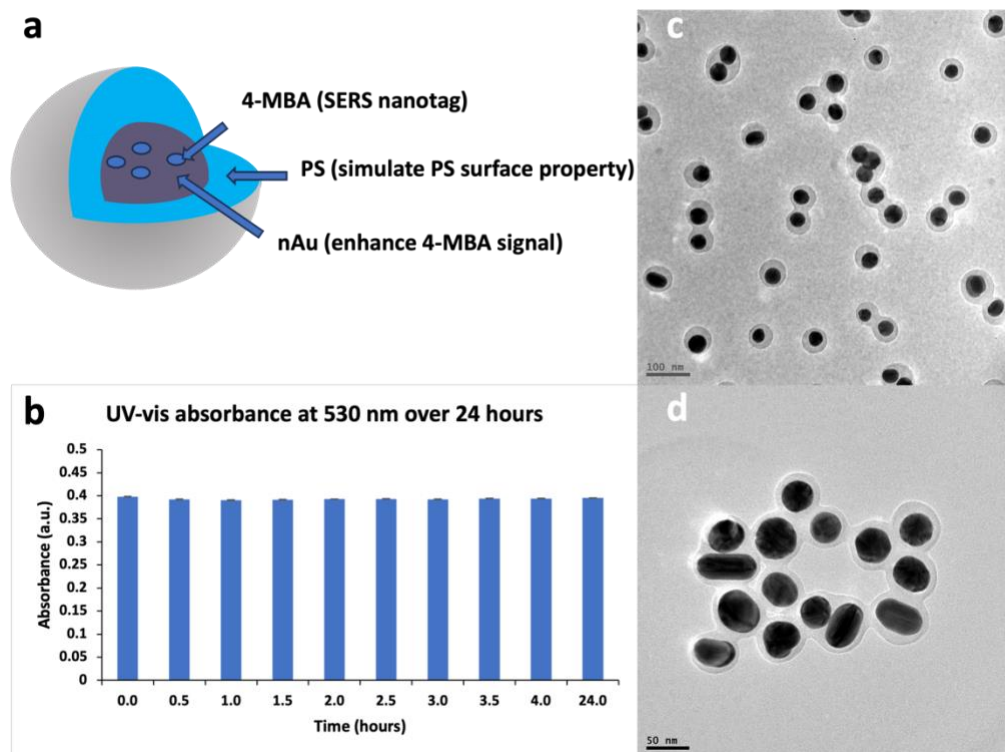

Fig. 1. Panel a shows the strucuter details of the model NP, and panel b displays the maximum absorption values over 24 hours at 530 nm. Panels c and d present TEM images of the freshly made model NPs and those after 12 months, respectively.

aggregate and settle quickly, we conducted a 24-hour UV-Vis test. The same suspension sample

remained in the cuvette for the entire 24-hour duration. The results demonstrated that the model NPs suspension was very stable with an absorbance of 0.39 ± 0.016 (**Fig. 1b**).

3.2 SERS limit of detection and calibration curve

A Raman spectroscope equipped with a confocal microscope was used in this study to obtain 2D/3D imaging of model NPs in garlic plants. The scanning speed is fast, with a low integration time of 0.001s/spectrum/pixel, and it provides high spatial resolution, reaching as small as 300 nm. The novel NP model enables multi-dimensional imaging through SERS and SERS has several unique advantages for NP imaging in biological samples, such as in-situ detection without causing damage to the living organism's matrix. This allows for the long-term study of biological samples to observe the uptake and distribution patterns of model NPs. Detecting model NPs with dye-free surfaces eliminates the need for fluorescent dye, thus avoiding any drawbacks associated with dyes. The model NP incorporates a nAu core that is labeled with a Raman indicator. The cores enhance Raman indicator signals, enabling the direct detection of model NPs through SERS. In contrast to traditional Raman spectroscopy, SERS has higher sensitivity by incorporating nAu cores, leading to a substantial increase in Raman signals by several orders of magnitude (10^5 - 10^{10})[31] To evaluate the sensitivity of SERS detection for the model NPs, the limit of detection was investigated. Since the model NPs can be dual-functionally detected by both SERS imaging and ICP-MS quantification, an SERS calibration curve was also created to complement and facilitate the results of ICP-MS quantification.

In order to calibrate the model PS concentrations and their Raman intensities, we prepared six concentrations of model PS suspension: 0 particles/mL, 1×10^9 particles/mL, 2×10^9 particles/mL, 2×10^{10} particles/mL, 1×10^{11} particles/mL, and 2×10^{11} particles/mL. We then applied 1µL of each concentration to foil and conducted SERS detection with five replicates for each concentration of

model PS suspension. The average Raman spectra for each concentration are displayed in **Fig. 2a**, and their calibration curve with a trend line of y= 622.75x – 1386.4 (R^2 = 0.5639) is shown in **Fig. 2b**. The calibration shows an exponential trend, where an increase in concentration results in an exponential rise in Raman intensity. This enables us to predict the concentration of model PS from the Raman intensity and helps facilitate the quantification results from ICP-MS.

To evaluate the detection limit of SERS for this model PS, a single particle detection by SERS was conducted to determine its feasibility. We first diluted the model PS suspension and used an indexed TEM grid to locate a single PS particle with TEM (**Fig. 2c**). Afterward, we subjected this single particle to Raman detection. However, due to the extremely small amount of model PS, the signal was not significantly enhanced. A very weak Raman intensity of 5.3 was detected using high laser power (**Fig. 2d**). The successful detection of the single model PS demonstrated the high sensitivity of SERS method and helped achieve reliable and accurate detection results.
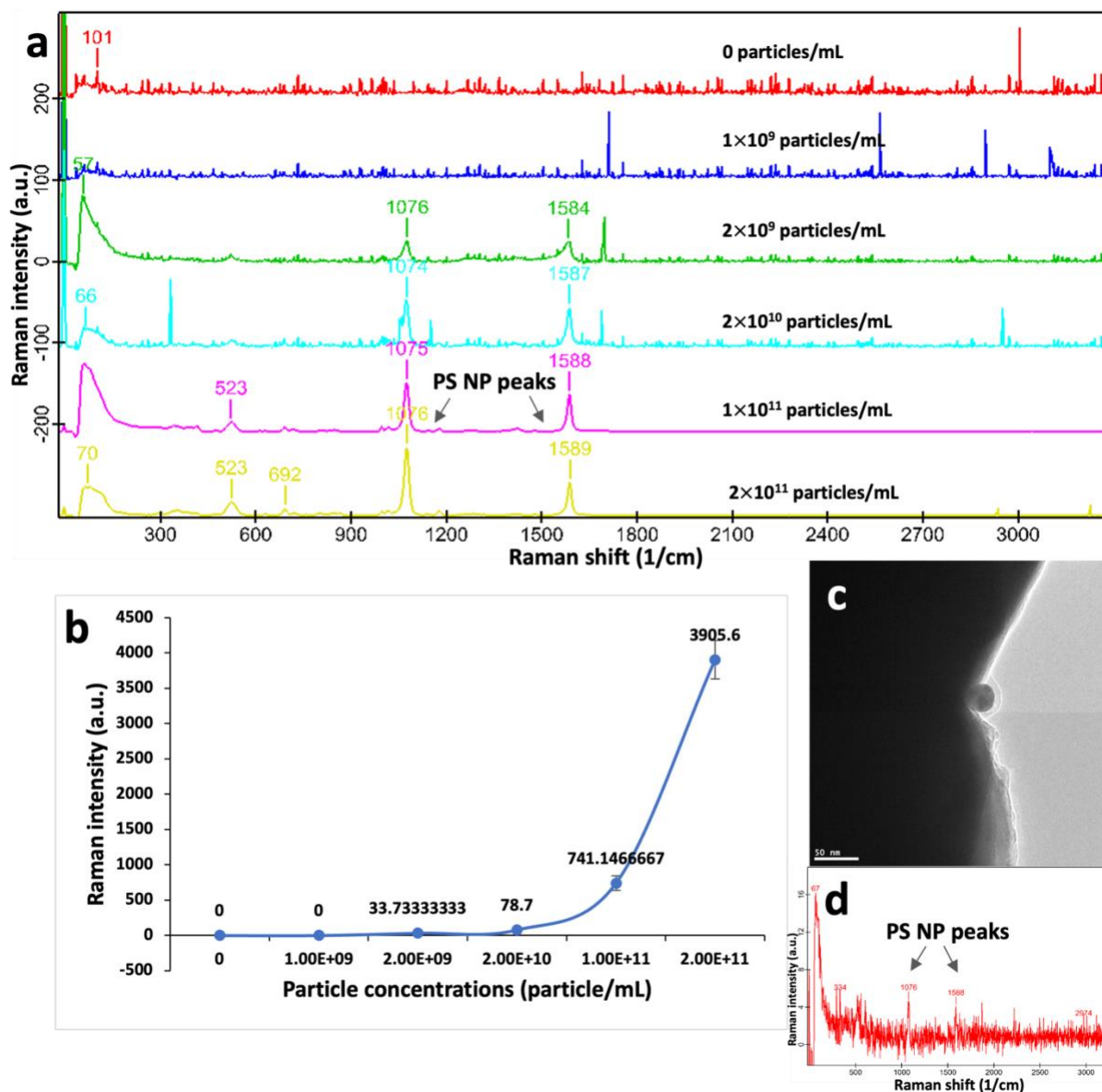
Fig. 2. Panel A shows the average Raman spectra of the model PS at six different concentrations on foil: 0 particles/mL, 1×10^9 particles/mL, 2×10^9 particles/mL, 2×10^{10} particles/mL, 1×10^{11} particles/mL, and 2×10^{11} particles/mL, respectively. Panel B displays the calibration of model NP concentrations and their corresponding Raman intensities. A single model PS NP was observed with TEM (panel c), and its detection using SERS is shown in panel d.

3.3 SERS imaging and ICP-MS quantification of model NPs in garlic roots

3.3.1 SERS imaging of various PS NP concentrations uptake in garlic roots

We aimed to explore the possibility of SERS imaging for detecting the model PS NPs in a garlic

plant matrix. To achieve this, we investigated the uptake of various concentrations of PS NP

suspensions in garlic plants using SERS imaging. By conducting a depth line scan on garlic plants with the confocal Raman microscope, we simulated a transection of the garlic plants, facilitating visualization of their cross-sectional morphology. Detection of PS NPs within the scanned region enables the characterization of their uptake via imaging techniques. We chose to scan the root tip region as
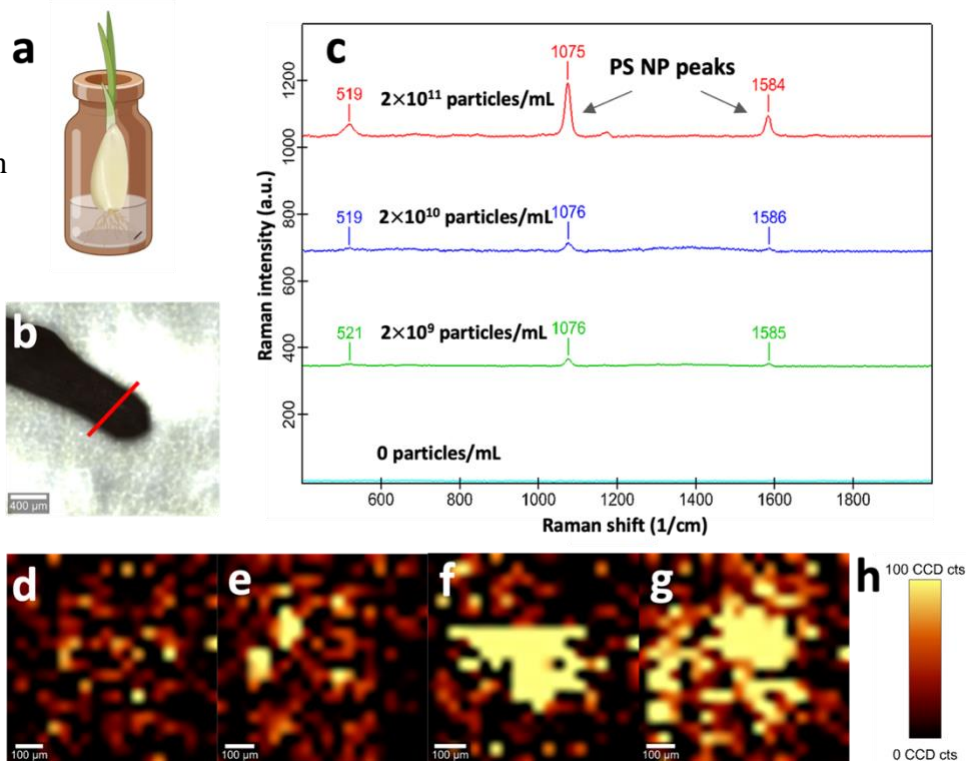

Fig. 3. Panel a shows the experimental setup involving a garlic plant placed in an amber vial containing a suspension of PS NPs. Panel b displays a microscopic image illustrating the location of a depth line scan performed on a garlic root. Panel c presents Raman intensity spectra of PS NPs obtained from garlic roots on day 30, demonstrating variations corresponding to different concentrations of PS NP suspension exposure. Their Raman maps at the characteristic peak of model NPs (1078 cm^{-1}) are shown in panels d-g, representing PS NP concentrations of 0 particles/mL, 2×10^9 particles/mL, 2×10^{10} particles/mL, and 2×10^{11} particles/mL respectively. The color scale bar is provided in panel h.

shown in **Fig. 3a, 3b**, as it experienced prolonged exposure to the PS NP suspensions since the beginning of the experiment. To assess the impact of varying concentrations of PS NP suspensions on PS NP uptake by garlic roots, we established three different concentration groups along with a control group (without PS NP exposure) to observe any variations. The confocal Raman depth line scan was performed on day 30, marking the end of the cultivation period. There are five replicates in each concentration group and the average Raman spectra of each group are shown in **Fig. 3c**. Upon examination of the Raman spectra, it was noticeable that as the concentrations of PS NPs increased, there was a corresponding rise in the average Raman

intensity observed on the garlic root tip regions as well. The Raman mappings at the characteristic peak of PS NPs (1078 cm^{-1}) are shown in panels d-g of **Fig. 3**. These mappings correspond to PS NP concentrations of 0 particles/mL, 2×10^9 particles/mL, 2×10^{10} particles/mL, and 2×10^{11} particles/mL respectively. By comparing these maps, we can observe the morphology of the cross-sectional area of the garlic root where signals of PS NPs are present. As we move from the control group towards lower concentrations of PS NP suspensions and then to higher concentrations, there is a notable increase in the pixels exhibiting signals. This further validates and aligns with the Raman spectra, as exposing garlic roots to higher concentrations of PS NP suspensions results in increased uptake of PS NPs.

3.3.2 SERS imaging of PS NP uptake over time in garlic roots

We tried to investigate whether prolonged exposure of garlic roots to PS NP suspensions results in increased uptake with SERS imaging. To ensure consistency, we chose to continue focusing on the garlic root tip region for this portion of the study. The garlic samples were from the concentration group of 2×10^{11} particles/mL, as the highest concentration group offers clearer and more pronounced imaging, allowing for better visualization of the differences in Raman imaging. We chose to conduct scans on garlic roots on three separate days: day 7, day 14, and day 30. To maintain reliability, we conducted three replicates each day, as there were only three garlic samples with roots available on day 7. This approach was essential to ensure timely scanning before the uptake occurred for too long. By looking at the Raman maps obtained from three different days, it is evident that the PS NPs were present since day 7 and persisted until day 30 in garlic roots (**Fig. 4c-e**). Upon comparing their Raman spectra and intensities, a clear trend emerges, indicating that with longer exposure to PS NPs, the average intensities significantly increased (**Fig. 4a-b**).
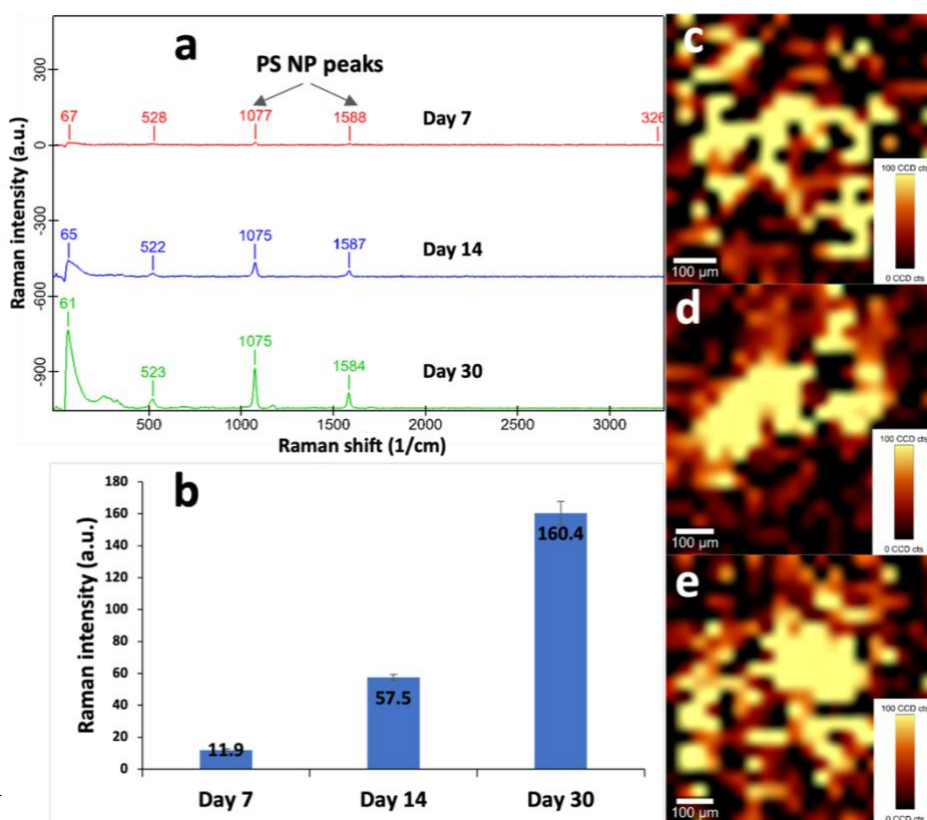

Fig. 4. Panel a presents the average Raman intensity spectra of PS NPs obtained from garlic roots on days, 14, and 30, demonstrating variations corresponding to different exposure times to PS NP suspensions. The specific Raman intensities are shown in panel b. Their Raman maps generated at the characteristic peak of model NPs (1078 cm⁻¹) are shown in panels c-e with a color scale bar, representing exposure time of day 7, day 14, and day 30 respectively.

This demonstrated that prolonged exposure to PS NPs allowed garlic roots to uptake a great quantity of PS NPs.

3.3.3 SERS imaging of PS NP uptake at different locations of garlic roots

Even though we have demonstrated that garlic roots possess the ability to uptake PS NPs into their roots in the previous study, we are still interested in investigating whether different locations on the root exhibit varying uptake capabilities. To accomplish this study, SERS imaging was conducted to visualize the distribution of PS NPs in roots. The garlic samples used were from the group with a concentration of 2×10^{11} particles/mL PS NP suspension. SERS scans were performed for all five replicates on the 30th day of garlic cultivation. The confocal Raman depth scans followed the same procedure, with the only variation being the direction of the line drawn for scanning. Instead of conducting the vertical scans as shown in **Fig. 5b**, we performed a horizontal scan as illustrated in **Fig. 5b**. This allowed for a larger area to be scanned, facilitating a
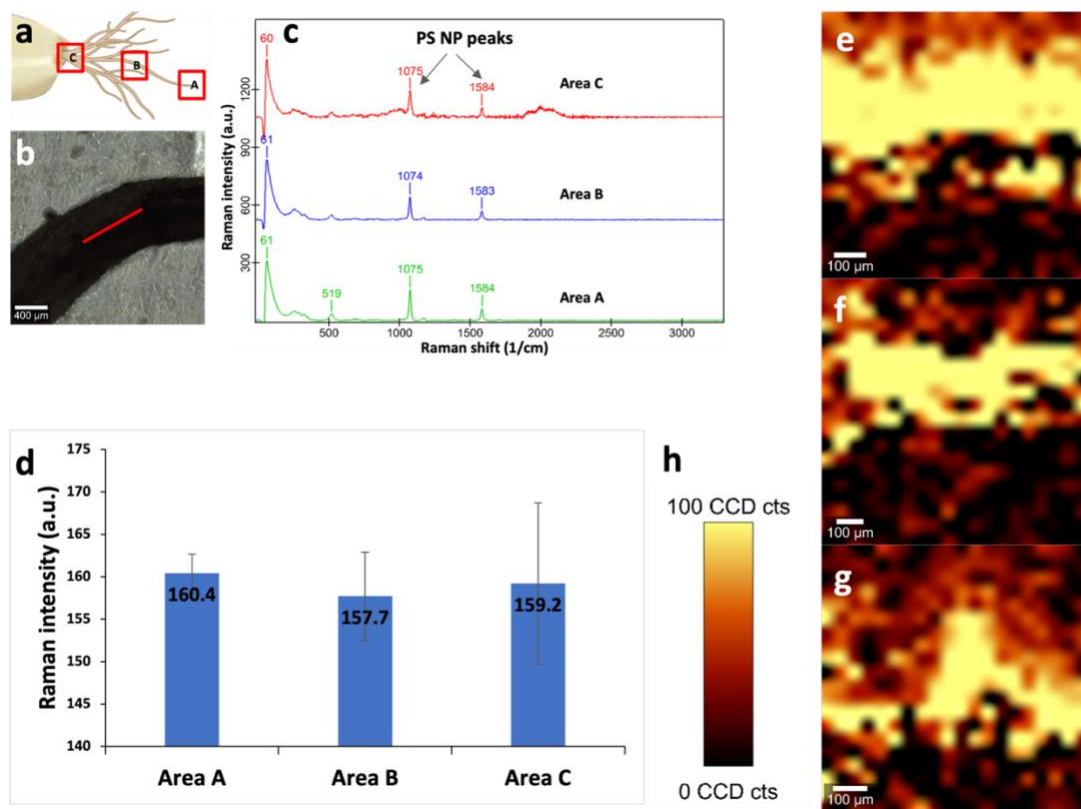

Fig. 5. Illustration of garlic roots with three labeled scanned areas is shown in panel a. Panel b shows the microscopic image of area B of a garlic root with a labeled depth scan line. Their average Raman spectra and Raman intensities of PS NPs are shown in panels c and d. Panels e-g represent the Raman mappings at the characteristic peak (1078 cm^{-1}) of areas A, B, and C respectively, with the color scale bar shown in panel h.

more extensive view of the root when imaging the distribution of PS NPs. Three locations were examined as shown in **Fig. 5a**, including the tip (A), the middle (B), and the top (C) parts. It appears that the uptake across the three locations is relatively consistent based on the average Raman intensity (**Fig. 5c-d**). The average intensity consistently displayed a uniform intensity level. Based on the results of the Raman maps, indications of PS NP presence were observed in all three locations with significant Raman intensities (**Fig. 5e-g**). In conclusion, all the findings suggest that different locations on the same root exhibit similar PS NP uptake abilities on day 30, however, the outcomes with shortened exposure durations are unknown.

3.3.4 ICP-MS quantification of the PS NP uptake within garlic plants

We aimed to assess whether the model NPs could be detected using ICP-MS by measuring their concentration in garlic plants with this technique. To quantitatively assess the distribution of PS NPs in different garlic parts, we used ICP-MS to quantify the uptake of PS NPs by the garlic plants. Figure 5a shows the procedure of ICP-MS samples
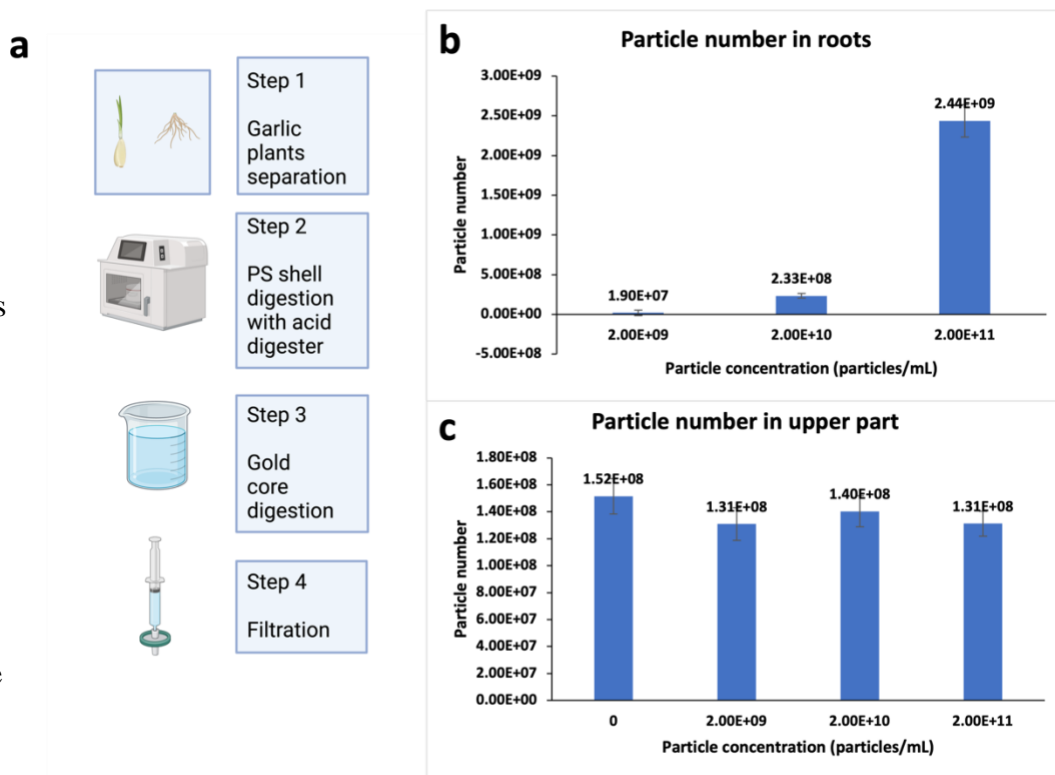

Fig. 6. Panel a illustrates the steps involved in preparing garlic plant samples for ICP-MS analysis, which includes acid digestion followed by sample filtration to ensure purity. Panel b displays the average number of NP particles detected in the roots of garlic plants across three different NP exposure concentration groups. Panel c illustrates the average number of NP particles detected in the upper parts of garlic plants for the same three concentrations groups, as well as a control group.

preparation. We first divided the garlic plants into two segments: the roots that were in constant contact with the PS NP suspension, and the upper part that was not in contact with the PS NPs in the vial. For the digestion of the PS shell and garlic tissue, a high-temperature and high-pressure acid digester was used in conjunction with an acid mixture. Additionally, aqua regia was used to digest the gold core at the center, and the process was performed at room temperature. Finally, a filtration step was carried out to remove impurities from the digested samples. By analyzing the numbers of PS NPs in these two segments, we can determine whether NPs transported from the roots to the upper part. The ICP-MS analysis results provide the gold concentration in parts per billion (ppb), represented as µg/L. Since the mass of each gold core in the PS NP is known, we could subsequently calculate the number of PS NPs in the analyzed garlic plants. By examining the final particle number results, we can observe a trend wherein garlic plants grown in varying concentrations of PS NP suspension exhibit a correlation: higher concentrations of PS NP suspension correspond to a great number of PS particles detected in the roots (**Fig. 6b**). ANOVA test was conducted for four groups, yielding a p-value of 0.042, indicating statistically significant differences among groups. For the 2×10^9 particles/mL and 2×10^{10} particles/mL PS NPs groups, the average particle numbers are slightly elevated compared to the control group. This can be attributed to the low concentration of PS NP suspensions. However, for the 2×10^{11} particles/mL group, there is a significant increase in particle numbers detected in roots, indicating that higher concentrations of PS NP suspensions lead to greater uptake of PS NPs by garlic roots.

To further investigate the uptake of PS NPs in garlic plants, the upper part of garlic which has never directly come into contact with PS NPs was analyzed using ICP-MS. Considering that the average height of the upper parts of garlic plants is 8.5 cm, and each line scan only covers less than 1000 µm, it lacks comprehensiveness to encompass the entirety of the upper parts, making

the PS NPs challenging to detect by SERS. However, the results for the control group, as well as for groups of 2×10^9 particles/mL, 2×10^{10} particles/mL, and 2×10^{11} particles/mL, exhibit similar results, indicating the absence of PS NPs within the upper part of garlic plants in these groups (**Fig. 6c**). One possible reason is that the number of PS NPs in the upper part of the garlic plant is too low, falling below the detection limit and therefore not detectable.

In summary, utilizing ICP-MS enabled us to accurately quantify PS NPs in the garlic roots, complementing the SERS imaging technique. Our findings demonstrated that exposure to higher concentrations of PS NP suspensions results in increased uptake by garlic plants in roots.

4. Conclusion

This study aimed to develop a dual-functional model NP and test its application in biological samples by investigating the uptake and distribution of model PS Ns in garlic plants. The development of this model material allows for a dual-functional analysis with the model PS NPs. This enables us to use both SERS imaging and ICP-MS quantification techniques to detect model NPs in garlic plants. The model PS NPs also address the challenge of collecting NPs from the environment without impurities.

Utilizing SERS imaging, we discovered that prolonged exposure to PS NPs resulted in increased uptake by garlic roots. Uptake was observed to start on day 7 and continued to escalate until the end of the 30-day study period. Other findings on day 30 also revealed that higher concentrations of PS NPs corresponded to increased uptake by roots. However, we also observed that three different locations on the root exhibited a similar number of uptake PS NPs on the 30th day. This finding is limited due to the extended exposure period. Results may have varied if tested earlier, and examining multiple concentration groups could yield different outcomes. Through ICP-MS quantification, we successfully detected the presence of model NPs in garlic plants roots. This

confirms the possibility of using ICP-MS to detect model NPs in living organism. With this model of PS NPs, we were also able to explore their effects on the growth of garlic plants. Based on the observations and results obtained from the 30-day cultivation of garlic plants, we found that exposing the PS NPs only once at the beginning did not result in any discernible negative or positive effects on garlic plant growth/germination during the cultivation period. All garlic plants across groups successfully germinated roots and shoots within 30 days, with no discernible difference in germination rates observed. However, if the exposure to PS NPs continued during the growth period, similar to what occurs in environmental scenarios such as NP-contaminated irrigation water continuously contacting the plants, a significantly lower germination rate was observed. Under the same growing conditions and watering intervals, the groups contaminated with PS NPs exhibited a maximum of 40% germinated rate (**Fig. S1-2**).

In future studies, continuous exposure to model NPs throughout the growth period may be considered to better replicate environmental scenarios, thus, the uptake by garlic plants might potentially be more obvious and easily detectable with both SERS and ICP-MS.

With the development of the dual-functional model material, we can replicate the behavior of NPs and their interactions with garlic plants, mirroring real-world conditions. By combining SERS imaging and ICP-MS, we successfully visualize and quantify the presence of PS NPs within garlic plants, enhancing the efficiency of our investigation. This research highlights the potential of using a combination of SERS and ICP-MS as a powerful analysis model for detecting dual-functional model PS NPs in agricultural samples. This could have significant implications for food safety and public health.

Acknowledgments

Conflict of Interest

The authors declare no competing interests.

(1) Andrady, A. L.; Neal, M. A. Applications and Societal Benefits of Plastics. *Philosophical Transactions of the Royal Society B: Biological Sciences* **2009**, *364* (1526), 1977–1984. https://doi.org/10.1098/rstb.2008.0304.

(2) Rizan, C.; Mortimer, F.; Stancliffe, R.; Bhutta, M. F. Plastics in Healthcare: Time for a Re-Evaluation. *Journal of the Royal Society of Medicine*. SAGE Publications Ltd February 1, 2020, pp 49–53. https://doi.org/10.1177/0141076819890554.

(3) Agarwal, S.; Gupta, R. K. Plastics in Buildings and Construction. *Applied Plastics Engineering Handbook: Processing, Materials, and Applications: Second Edition* **2017**, 635–649. https://doi.org/10.1016/B978-0-323-39040-8.00030-4.

(4) Andrady, A. L. Microplastics in the Marine Environment. *Mar Pollut Bull* **2011**, *62* (8), 1596–1605. https://doi.org/10.1016/J.MARPOLBUL.2011.05.030.

(5) Undas, A. K.; Groenen, M.; Peters, R. J. B.; van Leeuwen, S. P. J. Safety of Recycled Plastics and Textiles: Review on the Detection, Identification and Safety Assessment of Contaminants. *Chemosphere* **2023**, *312*, 137175. https://doi.org/10.1016/J.CHEMOSPHERE.2022.137175.

(6) Rodrigues, M. O.; Abrantes, N.; Gonçalves, F. J. M.; Nogueira, H.; Marques, J. C.; Gonçalves, A. M. M. Impacts of Plastic Products Used in Daily Life on the Environment and Human Health: What Is Known? *Environ Toxicol Pharmacol* **2019**, *72*, 103239. https://doi.org/10.1016/J.ETAP.2019.103239.

(7) Geyer, R.; Jambeck, J. R.; Law, K. L. *Production, Use, and Fate of All Plastics Ever Made*; 2017. https://www.science.org.

(8) Subramanian, P. M. Plastics Recycling and Waste Management in the US. *Resour Conserv Recycl* **2000**, *28* (3–4), 253–263. https://doi.org/10.1016/S0921-3449(99)00049-X.

(9) Sun, J.; Zheng, H.; Xiang, H.; Fan, J.; Jiang, H. The Surface Degradation and Release of Microplastics from Plastic Films Studied by UV Radiation and Mechanical Abrasion. *Science of The Total Environment* **2022**, *838*, 156369. https://doi.org/10.1016/J.SCITOTENV.2022.156369.

(10) Cai, L.; Wang, J.; Peng, J.; Wu, Z.; Tan, X. Observation of the Degradation of Three Types of Plastic Pellets Exposed to UV Irradiation in Three Different Environments.

Science of The Total Environment **2018**, *628–629*, 740–747. https://doi.org/10.1016/J.SCITOTENV.2018.02.079.

(11) Roager, L.; Sonnenschein, E. C. Bacterial Candidates for Colonization and Degradation of Marine Plastic Debris. *Environmental Science and Technology*. American Chemical Society October 15, 2019, pp 11636–11643. https://doi.org/10.1021/acs.est.9b02212.

(12) Shah, A. A.; Hasan, F.; Hameed, A.; Ahmed, S. Biological Degradation of Plastics: A Comprehensive Review. *Biotechnol Adv* **2008**, *26* (3), 246–265. https://doi.org/10.1016/J.BIOTECHADV.2007.12.005.

(13) Revel, M.; Châtel, A.; Mouneyrac, C. Micro(Nano)Plastics: A Threat to Human Health? *Curr Opin Environ Sci Health* **2018**, *1*, 17–23. https://doi.org/10.1016/J.COESH.2017.10.003.

(14) Materić, D.; Peacock, M.; Dean, J.; Futter, M.; Maximov, T.; Moldan, F.; Röckmann, T.; Holzinger, R. Presence of Nanoplastics in Rural and Remote Surface Waters. *Environmental Research Letters* **2022**, *17* (5). https://doi.org/10.1088/1748-9326/ac68f7.

(15) Zhang, Y.; Gao, T.; Kang, S.; Shi, H.; Mai, L.; Allen, D.; Allen, S. Current Status and Future Perspectives of Microplastic Pollution in Typical Cryospheric Regions. *Earth Sci Rev* **2022**, *226*, 103924. https://doi.org/10.1016/J.EARSCIREV.2022.103924.

(16) Wang, Y. L.; Lee, Y. H.; Chiu, I. J.; Lin, Y. F.; Chiu, H. W. Potent Impact of Plastic Nanomaterials and Micromaterials on the Food Chain and Human Health. *International Journal of Molecular Sciences*. MDPI AG March 1, 2020. https://doi.org/10.3390/ijms21051727.

(17) Lai, H.; Liu, X.; Qu, M. Nanoplastics and Human Health: Hazard Identification and Biointerface. *Nanomaterials*. MDPI April 1, 2022. https://doi.org/10.3390/nano12081298.

(18) He, D.; Luo, Y.; Lu, S.; Liu, M.; Song, Y.; Lei, L. Microplastics in Soils: Analytical Methods, Pollution Characteristics and Ecological Risks. *TrAC Trends in Analytical Chemistry* **2018**, *109*, 163–172. https://doi.org/10.1016/J.TRAC.2018.10.006.

(19) He, D.; Zhang, Y.; Gao, W. Micro(Nano)Plastic Contaminations from Soils to Plants: Human Food Risks. *Curr Opin Food Sci* **2021**, *41*, 116–121. https://doi.org/10.1016/J.COFS.2021.04.001.

(20) Sun, X. D.; Yuan, X. Z.; Jia, Y.; Feng, L. J.; Zhu, F. P.; Dong, S. S.; Liu, J.; Kong, X.; Tian, H.; Duan, J. L.; Ding, Z.; Wang, S. G.; Xing, B. Differentially Charged Nanoplastics Demonstrate Distinct Accumulation in Arabidopsis Thaliana. *Nat Nanotechnol* **2020**, *15* (9), 755–760. https://doi.org/10.1038/s41565-020-0707-4.

(21) Sun, H.; Lei, C.; Xu, J.; Li, R. Foliar Uptake and Leaf-to-Root Translocation of Nanoplastics with Different Coating Charge in Maize Plants. *J Hazard Mater* **2021**, *416*, 125854. https://doi.org/10.1016/J.JHAZMAT.2021.125854.

(22) Liu, Y.; Guo, R.; Zhang, S.; Sun, Y.; Wang, F. Uptake and Translocation of Nano/Microplastics by Rice Seedlings: Evidence from a Hydroponic Experiment. *J Hazard Mater* **2022**, *421*, 126700. https://doi.org/10.1016/J.JHAZMAT.2021.126700.

(23) Jiang, M.; Wang, B.; Ye, R.; Yu, N.; Xie, Z.; Hua, Y.; Zhou, R.; Tian, B.; Dai, S. Evidence and Impacts of Nanoplastic Accumulation on Crop Grains. *Advanced Science* **2022**, *9* (33). https://doi.org/10.1002/advs.202202336.

(24) Shen, M.; Zhang, Y.; Zhu, Y.; Song, B.; Zeng, G.; Hu, D.; Wen, X.; Ren, X. Recent Advances in Toxicological Research of Nanoplastics in the Environment: A Review. *Environmental Pollution* **2019**, *252*, 511–521. https://doi.org/10.1016/J.ENVPOL.2019.05.102.

(25) Snipstad, S.; Hak, S.; Baghirov, H.; Sulheim, E.; Mørch, Ý.; Lélu, S.; von Haartman, E.; Bäck, M.; Nilsson, K. P. R.; Klymchenko, A. S.; de Lange Davies, C.; Åslund, A. K. O. Labeling Nanoparticles: Dye Leakage and Altered Cellular Uptake. *Cytometry Part A* **2017**, *91* (8), 760–766. https://doi.org/10.1002/cyto.a.22853.

(26) Bakht, B. K.; Iftikhar, M.; Gul, I.; Ali, M. A.; Shah, G. M.; Arshad, M. Effect of Nanoparticles on Crop Growth. *Nanomaterials for Soil Remediation* **2021**, 183–201. https://doi.org/10.1016/B978-0-12-822891-3.00009-8.

(27) Lakshmikanthan, D.; Chandrasekaran, N. The Effect of Humic Acid and Polystyrene Fluorescence Nanoplastics on Solanum Lycopersicum Environmental Behavior and Phytotoxicity. *Plants* **2022**, *11* (21). https://doi.org/10.3390/plants11213000.

(28) Li, Z.; Feng, C.; Wu, Y.; Guo, X. Impacts of Nanoplastics on Bivalve: Fluorescence Tracing of Organ Accumulation, Oxidative Stress and Damage. *J Hazard Mater* **2020**, *392*, 122418. https://doi.org/10.1016/J.JHAZMAT.2020.122418.

(29) Liu, S.; Shang, E.; Liu, J.; Wang, Y.; Bolan, N.; Kirkham, M. B.; Li, Y. What Have We Known so Far for Fluorescence Staining and Quantification of Microplastics: A Tutorial Review. *Frontiers of Environmental Science and Engineering*. Higher Education Press Limited Company January 1, 2022. https://doi.org/10.1007/s11783-021-1442-2.

(30) Luo, Y.; Li, L.; Feng, Y.; Li, R.; Yang, J.; Peijnenburg, W. J. G. M.; Tu, C. Quantitative Tracing of Uptake and Transport of Submicrometre Plastics in Crop Plants Using Lanthanide Chelates as a Dual-Functional Tracer. *Nat Nanotechnol* **2022**, *17* (4), 424–431. https://doi.org/10.1038/s41565-021-01063-3.

(31) Guo, H.; He, L.; Xing, B. Applications of Surface-Enhanced Raman Spectroscopy in the Analysis of Nanoparticles in the Environment. *Environmental Science: Nano*. Royal Society of Chemistry 2017, pp 2093–2107. https://doi.org/10.1039/c7en00653e.

(32) Das, A.; Terry, L. R.; Sanders, S.; Yang, L.; Guo, H. Confocal Surface-Enhanced Raman Imaging of the Intestinal Barrier Crossing Behavior of Model Nanoplastics in Daphnia Magna. *Environ Sci Technol* **2024**. https://doi.org/10.1021/acs.est.3c10549.

(33) Materić, D.; Peacock, M.; Dean, J.; Futter, M.; Maximov, T.; Moldan, F.; Röckmann, T.; Holzinger, R. Presence of Nanoplastics in Rural and Remote Surface Waters. *Environmental Research Letters* **2022**, *17* (5). https://doi.org/10.1088/1748-9326/ac68f7.